1. Report No. UI-23-RP-02	2. Government Accession No N/A	3. Recipient's Catalog No. N/A
4. Title and Subtitle Innovative Precast Concrete Truss Using Adaptive Shape Memory Prestressing System		5. Report Date March 2026 6. Performing Organization Code N/A
7. Author(s) Bassem Andrawes, Ph.D., P.E., F.ASCE, (https://orcid.org/0000-0002-8954-3751) Alexander Chen, (https://orcid.org/0009-0002-0657-4323)		8. Performing Organization Report No. UI-23-RP-02
9. Performing Organization Name and Address University of Illinois Urbana-Champaign Department of Civil and Environmental Engineering Newmark Civil Engineering Laboratory, MC-250 205 North Mathews Ave. Urbana, IL 61801		10. Work Unit No. N/A 11. Contract or Grant No. 69A3552348333
12. Sponsoring Organization Name and Address Transportation Infrastructure Precast Innovation Center (TRANS-IPIC) University of Illinois Urbana-Champaign. Civil & Environmental Engineering. 205 N Mathews Ave, Urbana, IL 61801 US Department of Transportation Office of Research, Development and Technology (RD&T) 1200 New Jersey Avenue, SE Washington, DC 201590		13. Type of Report and Period Covered Final Report August, 2023 – December, 2025 14. Sponsoring Agency Code N/A
15. Supplementary Notes For additional reports and information, visit the TRANS-IPIC website https://trans-ipic.illinois.edu		
16. Abstract Material usage in transportation infrastructure can be optimized through the use of truss-based concrete bridge girders. The durability of the concrete members can be further enhanced with shape memory alloy (SMA) prestressing. These concepts were demonstrated using finite element analysis, and the truss girder reduced concrete volume by 37.3% when compared with a conventional girder. The SMA prestressing was experimentally proven for mortar, fiber reinforced concrete (FRC), and ultra high performance concrete (UHPC). SMA was also experimentally demonstrated for healing concrete by closing cracks upon activation. Crack widths in mortar, FRC, and UHPC were reduced by up to 80%, 90%, and 84%, respectively. A large-scale test of a truss girder with SMA was conducted, and the SMA successfully delayed cracking.		
17. Key Words Shape memory alloys (SMA); shape memory effect (SME); precast concrete; prestressing; optimization; bridge girder; truss; induction heating; healing; cracks		18. Distribution Statement No restrictions.
19. Security Classification (of this report) Unclassified.	20. Security Classification (of this page) Unclassified.	21. No. of Pages 32 / 22. Price N/A

Disclaimer:
The contents of this report reflect the views of the authors, who are responsible for the facts and the accuracy of the information presented herein. This document is disseminated in the interest of information exchange. The report is funded, partially or entirely, under 69A3552348333 from the U.S. Department of Transportation's University Transportation Centers Program. The U.S. Government assumes no liability for the contents or use thereof.

Transportation Infrastructure Precast Innovation Center (TRANS-IPIC)

University Transportation Center (UTC)

Innovative Precast Concrete Truss Using Adaptive Shape Memory Prestressing System

Project No.: UI-23-RP-02

FINAL REPORT

Submitted by:
Bassem Andrawes (PI), Ph.D., P.E., F.ASCE (andrawes@illinois.edu)
Proferssor
Department of Civil and Environmental Engineering
University of Illinois at Urbana-Champaign

Alexander Chen
Graduate Research Assistant
Department of Civil and Environmental Engineering
University of Illinois at Urbana-Champaign

Submitted to:
TRANS-IPIC UTC
University of Illinois Urbana-Champaign
Urbana, IL

Executive Summary:

The durability and material usage in transportation infrastructure can be improved through the use of optimized geometries and novel prestressing techniques. In this research project, the optimization of geometry was demonstrated through the development of bridge girders with truss systems for the webs. These girders transfer the loads in a more efficient manner and reduce the amount of concrete consumption per girder. The structural performance of these optimized girders can be further improved through the use of prestressing with shape memory alloys (SMAs). SMAs are a class of alloys with the ability to recover from inelastic deformation if exposed to heat. Heating (activation) of prestrained SMAs inside the concrete prestresses the concrete. This localized prestressing is ideal for the short, tensile members in the truss system. This improves the durability of the structure by delaying the onset of cracking in the concrete. Alternatively, the SMAs can also be activated after cracking has occurred. Doing so causes the SMAs to close the cracks and heal the concrete. This research explores these concepts in the form of six tasks. The first two tasks focused on the validation of the concepts through numerical modeling. The remaining four tasks focused on validation through experimental testing.

Two finite element (FE) models of bridges were created for Task 1. One bridge used the American Association of State Highway and Transportation Officials (AAHSTO) type II girders, and the other used a modified girder with truss-shaped webs and with SMA prestressing. Both bridges were evaluated for strength and service limit states. The truss girder was able to satisfy the limits while using less concrete than the type II girder, thereby validating the concept. Task 2 focused on optimizing the girder in the form of a parametric study. Different dimensions and reinforcement options were explored, and an optimized truss girder was developed.

The third task focused on combining SMA prestressing with other types of concrete that have higher crack resistance. Small-scale beam specimens were cast using mortar, fiber-reinforced concrete (FRC), and ultra-high performance concrete (UHPC). Activation of the SMA prior to cracking developed compressive forces that prestressed all three types of concrete. Activation of the SMA after cracking triggered crack closure. In the case of mortar, the crack width reduction was as high as 80%. In the FRC, crack width reduction was as high as 90%. In the UHPC, crack width reduction was as high as 84%. The fourth task focused on testing a flexural beam specimen reinforced with SMA bars with hooked ends. Crack closure was seen upon activation of the embedded SMAs. Task five focused on a test specimen designed for tensile loading. Activation of the SMAs prior to loading produced prestressing forces in the specimen. Activation after loading led to full crack closure.

The final task focused on combining results from the previous tasks into a large-scale test. A truss was cast based on the dimensions of the optimized truss in Task 2. One of the tensile members was reinforced with SMAs in a manner similar to Task 5. The SMAs were activated using an induction heater, and prestressing was captured using strain gauges. The truss was then loaded in three-point bending, and digital image correlation (DIC) was used to detect cracks. The tensile member with conventional steel reinforcement cracked before the member with SMA prestressing, thereby validating the use of SMAs in this manner. In conclusion, the concept of truss systems for bridge girders was demonstrated numerically and experimentally. The use of SMA prestressing for the tensile members of the truss was also successfully demonstrated. Together, these techniques can be used to improve the efficiency and durability of future transportation infrastructure.

Table of Contents

1. Problem description

Our current transportation infrastructure can be improved by reducing material use while increasing its durability. One approach to reducing concrete consumption is to employ geometrically optimized (truss) systems. This research addresses this need by developing and validating truss-based bridge girders. The durability of the girder is improved by using prestressing with shape memory alloys (SMAs). The SMAs allow for localized prestressing and eliminate the need for mechanical tensioning and special equipment. The research includes numerical simulation as well as fabrication and testing of truss structures reinforced with SMAs. This research also investigates the use of SMAs to close cracks (heal) concrete. This repair method requires no additional material to restore stiffness and improve durability.

2. Background

The current United States transportation infrastructure is deteriorating, with 6.7% of bridges labelled as “poor” condition (U.S. DOT, 2025). These bridges lead to reduced bridge weight limits, detours, and increased travel times (U.S. DOT, 2019). This situation presents a unique opportunity to introduce improved bridge designs to optimize efficiency nationwide. In recent years, researchers have used topological optimization techniques to generate new geometries that can utilize material more efficiently (Amir & Shakour, 2018; Menna & Esposito, 2022; Sung & Andrawes, 2023). However, a drawback of these geometries is the presence of complex cavities that are difficult to construct from concrete. Trusses are a better geometry for balancing efficiency and ease of construction. As shown in **Fig. 1**, a truss transforms a single bending beam into a series of tension and compression elements. Compared to topology optimization designs, the void shapes and sizes in trusses are more uniform, making them easier to manufacture. Concrete truss girders have been successfully built in several countries. In China, there is the Dongpo South Bridge, which uses prestressed steel truss webs (Benaim, 2008). In Japan, there is the Bessodani Bridge, which uses a double Warren truss made of concrete reinforced with prestressed aramid fiber reinforced polymer rods (Zerin & Kasuga, 2022). Some researchers have built trusses without prestressing by encasing concrete in steel tubing (Fong et al., 2011; Zhou et al., 2017). The steel increases the tensile strength of the components but leaves the steel exposed to the elements. A better approach is to prestress the concrete using internal reinforcing steel. Therefore, this research aimed at developing concrete trusses using innovative prestressing based on shape memory alloys (SMAs).

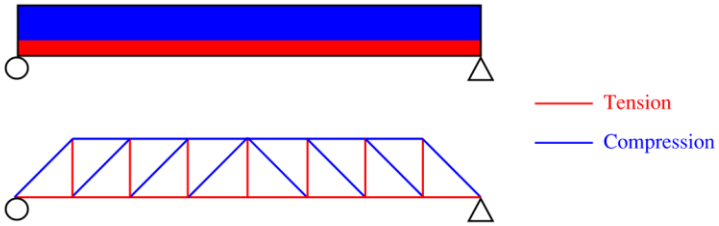

Fig. 1. Internal tension and compression forces.

2.1 Concrete crack control

Truss bridges have been constructed using a variety of materials. The earliest truss bridges were built from wood. Later, wrought iron truss bridges appeared in the 1700s (James, 1980). Today, truss bridges around the world are constructed of steel. The world's longest continuous steel truss bridge is the Ikuzuki Bridge in Japan, with a span of 1,312 feet (Doboku Gakkai, 1990). Historically, concrete is less commonly used in truss bridge construction. While concrete possesses excellent compressive strength, fire resistance, and corrosion resistance, it has relatively low tensile strength and is prone to cracking. These cracks expose the reinforcing steel

to environmental factors and cause corrosion (Lopez-Calvo et al., 2018; Otieno et al., 2010; Poursaee & Ross, 2022). Corrosion of the reinforcing steel exacerbates cracking and can cause concrete spalling. **Fig. 2** illustrates examples of such cracking. Over the years, various methods have been developed to control concrete cracking. A common approach is to delay crack initiation through prestressing. Traditional prestressing methods apply constant stress to concrete using stretched tensile steel reinforcement (Menn, 2012). However, prestressing the tension members of concrete truss girders in this way is challenging due to the intersections with the bottom chord. Therefore, this study explored an alternative prestressing method using SMAs to achieve more targeted prestressing. This prestressing method relies on heating the SMA above its transition temperature after it has been inserted into the concrete. The study experimentally verified the application of SMA prestressing in conventional precast concrete as well as in fiber reinforced and ultra-high performance concrete.

Fig. 2. Cracks underneath concrete bridges (Andrawes et al., 2024).

Another crack control method is to repair the crack after it has appeared. This typically involves filling the crack with grout (ACI, 2007) or epoxy (Kim & Park, 2021). These methods have limitations, such as needing to clean out the crack beforehand (ACI, 2008). Using epoxy resin also requires extra care, as it needs to fully penetrate the crack to achieve optimal results (Griffin et al., 2017). Another crack control method is to use "self-healing" concrete. This method does not require adding material to the crack. Instead, the concrete itself fills the crack. This is achieved by adding microcapsules containing a healing agent during the concrete mixing process. When the concrete cracks, the microcapsules rupture, releasing the healing agent and filling the crack (Z. Yang et al., 2010). However, none of the above methods can pull the sides of the crack back to their original position, meaning that dislocations still exist in the structure after repair. This study explored a novel SMA-based healing method, with the unique goal of completely closing cracks.

Aside from prestressing, another method for crack control is to employ concrete mix designs with better crack resistance. Fiber-reinforced concrete (FRC) is one such mix design, incorporating fibers during the mixing process to enhance crack resistance (Van Chanh, 2004; C. Zhao et al., 2023; Zollo, 1997). Ultra-high performance concrete (UHPC) is another type of concrete that also uses fibers to improve crack resistance. UHPC also exhibits significantly higher compressive strength than conventional concrete. The Federal Highway Administration (FHWA) defines the minimum compressive strength of UHPC as 17.5 ksi (Graybeal & El-Helou, 2023). These properties have led to the widespread use of UHPC in various bridge applications. It has been used in superstructures (Benjamin Graybeal, 2009) and for the repair of bridge components (Haber et al., 2022). These properties make both FRC and UHPC ideal materials for tension members of concrete truss girders. There is, however, one drawback to using UHPC. It has poor fire resistance and reacts with explosive spalling (Chen et al., 2020). This presents a problem because shape memory alloys (SMAs) require heating to develop their recovery stresses. Therefore, this study investigated two different heating methods to determine which is best suited for safely activating SMAs embedded in FRC and UHPC. The first method involves heating the SMA by passing an electric current through it. Park & Andrawes (2025) have used this method to

successfully heat SMA in conventional concrete. A disadvantage to this method is that it requires exposing the ends of the SMA, reducing its efficiency because the exposed portions do not contribute any prestressing when activated. Another method involves adding lead wires to the SMAs. However, these wires can impede the flow of concrete during pouring, potentially leading to voids and weakening the concrete. An induction heater avoids these issues because magnetic waves can penetrate concrete. Therefore, this research used an induction heater as the second method for heating SMA inside of FRC and UHPC.

2.2 Shape memory alloys

The first shape memory alloy developed was a nickel-titanium-based alloy discovered at the U.S. Naval Ordnance Laboratory in the 1960s. It exhibited a unique ability to return from a deformed state to its original shape upon heating. This phenomenon, known as the shape memory effect (SME), is due to the crystal structure transformation of the SMA between martensite and austenite phases (Gallardo Fuentes et al., 2002; Lagoudas, 2008). The SME only occurs when the SMA reaches a critical transformation temperature. If the SMA is constrained and heated above its transformation temperature, the SME generates "recovery stress" (**Fig. 3**). This recovery stress in some alloys persists after the SMA cools, making it a practical property for civil engineering. The recovery stress of prestrained SMA wires has been extensively studied (Choi et al., 2012; Dommer & Andrawes, 2012). By adding the prestrained SMA wires into concrete during casting and then heating the SMA after curing, the SMA will generate prestress within the concrete. Sung & Andrawes (2021) experimentally validated this concept by wrapping NiTiNb wires within nylon sleeves and embedding them into concrete rail ties. The wires were then heated, generating localized prestress in key areas of the ties. Researchers have used similar techniques to fabricate precast plates for the repair of existing concrete structures (Gunasekaran et al., 2025; H. Zhao & Andrawes, 2020). Another method for achieving stress recovery in concrete using SMAs involves winding prestressed SMA wires around columns. Upon heating, the wires generate active confinement and improve the structural performance of the columns (Andrawes et al., 2009). SMAs can also be used to reinforce steel structures. Researchers have attached prestrained SMA strips to an old bridge and heated them to prestress and repair the girders (Vůjtěch et al., 2021).

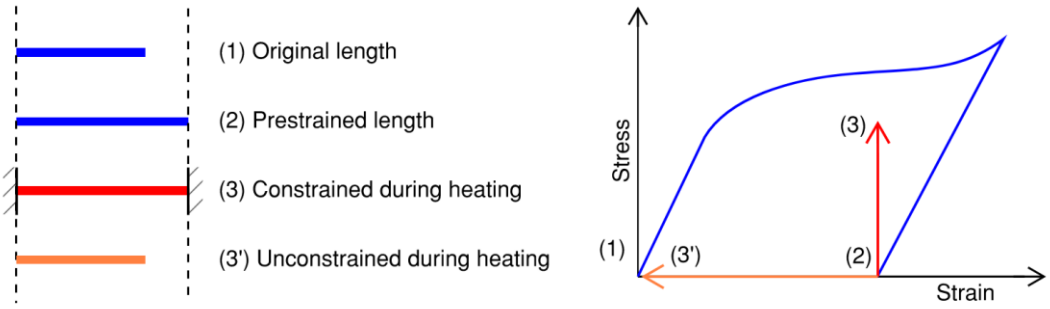

Fig. 3. Shape memory effect and recovery stress in SMAs

3. Research scope and objectives:

This research aimed at addressing how to design and fabricate concrete truss structures reinforced with SMAs. To this end, the research plan focused on six tasks. The first two tasks focused on designing specimens using the finite element (FE) method. The FE analysis was carried out in the software ABAQUS. The aim was to find the optimal placement of SMA for localized prestressing to control cracking. Task 1 includes modeling a full bridge to assess the performance with AASHTO limit states. A second bridge of conventional steel reinforcement was used as a baseline. Task 2 focused on modeling only the girder to develop a design that can be

easily fabricated and tested. The remaining tasks were directed towards the fabrication, instrumentation, and testing of different specimens. In Task 3, a study was conducted on the performance of SMA bars in different types of concrete. The SMA bars were prestrained and then activated in small-scale specimens to either prestress or heal the concrete. Tasks 4 and 5 studied the performance of SMA bars inside specimens subjected to flexural and tensile loading, respectively. Finally, Task 6 involved fabricating and testing a large-scale concrete truss to validate the concept. Conventional instrumentation and digital image correlation (DIC) were used to evaluate the performance of the truss.

4. Research description, results, and conclusion:

4.1 Design of Full-scale Truss Bridge using Finite Element Method

This study used FE analysis to analyze a full-scale bridge with a concrete truss girder design. The design was based on a Howe truss for simplicity. This places the bottom chord and vertical members in tension, and the top chord and diagonals in compression. Concrete is weak in tension, so prestressing was introduced in the tensile members. The bottom chord was prestressed with mechanical tensioning, and the verticals were prestressed with SMA bars. The FE results were used to evaluate the bridge under AASHTO limit states. The girder was also compared with a conventional AASHTO girder design to assess differences in material consumption.

An example bridge was developed to represent a typical single-span mid-range bridge (**Fig. 4(a)**). The deck was 8 inches thick and supported by five AASHTO Type II girders spaced 8 feet apart. The bridge was 40 feet wide and spanned 60 feet. A second bridge was designed by changing the girders of the example bridge into trusses (**Fig. 4(b)**). The design used the truss analogy, in which the top chord and diagonal members are in compression, while the bottom chord and vertical members are in tension. The number of girders and spacing were the same for both bridges (**Fig. 4(c)**). The profile of the truss girder is similar to the AASHTO type II girder (**Fig. 4(d)**) but with the height increased to 42 inches and the lower flange reduced to the same width as the top (**Fig. 4(e)**). Triangular voids in the web region were used to remove excess concrete and form the truss shape. The diagonal members are angled at 45° for simplicity, and a 4-inch radius was added to the joints to prevent unnecessary stress concentration (**Fig. 4(f)**). The concrete truss is prestressed using both shape memory alloys (SMAs) and a conventional prestressing system. The capacity of conventional prestressing steel is higher than that of SMA, so it is more appropriate for the bottom chord. The vertical members carry less force and are better suited for SMAs. Unlike the bottom chord, prestressing of the vertical members is more challenging due to their shorter length and the large number of members. The SMA hoops eliminate the need for additional anchors and additional use of hydraulic jacking systems. The proposed concrete truss system can be manufactured in a process similar to conventional precast prestressed concrete. First, non-prestressed steel bars and SMA bars are installed in pre-determined positions within a mold. A hydraulic jacking system is used to pre-tension the prestressed steel bars in the bottom chord. Then, concrete is poured and cured. The pre-tensioned steel bars are released, prestressing the lower chord. Finally, the embedded SMA steel bars are heated to prestress the vertical members.

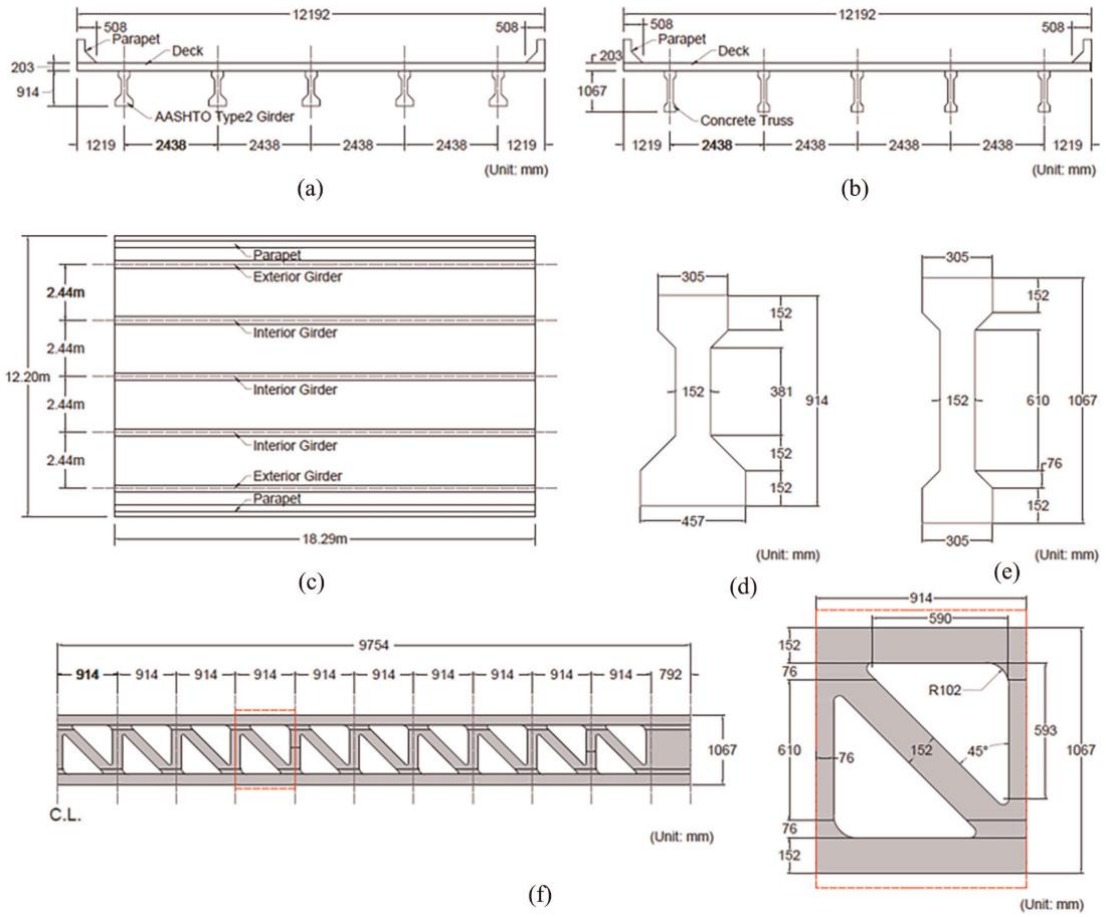

Fig. 4. Cross-section of (a) reference bridge using AASHTO type 2 girder, (b) concrete truss bridge, (c) plan-view of bridge models, cross-section of (d) AASHTO type 2 girder, (e) concrete truss, and (f) elevation of concrete truss.

Both the reference bridge and the concrete truss bridge were designed to satisfy the AASHTO Strength I Limit States (AASHTO, 2024). The reference bridge used seven-wire strands with a diameter of 0.6 inches. Twelve strands are at the bottom of the section, and two are at the top (**Fig. 5(a) and (c)**). The shear reinforcement is No. 5 Grade 60 steel bars spaced at 6 inches. The concrete truss bridge has six 0.6-inch diameter strands in the bottom (**Fig. 5(b) and (d)**). Each vertical member was reinforced with two non-prestressed steel bars and one 0.6-inch diameter SMA bar. The models were analyzed in ABAQUS (Dassault Systèmes Simulia Corp., 2011). By taking advantage of structural symmetry, only a quarter of each bridge needed to be modeled. Semicircular support pins were set at the ends. The girders and decks were meshed using 8-node cube elements and modeled using a concrete damage plasticity material model with compressive strengths of 8 ksi and 5 ksi, respectively. The steel reinforcement was meshed using 2-node truss elements and modeled using elastoplastic material models. The SMA bars were modeled as truss elements, using an elastoplastic material model derived from material test results. The steel and SMA were embedded in the concrete using the embedded region constraint. The FE analysis was conducted in three stages: prestressing, composite, and bending. In the prestressing stage, only the girder is active. This simulated the initial construction stage, where the beam was cast but not yet transported to the site. Prestress in the HSS steel strands was applied by releasing the pre-tensioned strands, while prestress in the SMA was applied by heating. The beam's self-weight, with a load factor of 1.25, was applied as a distributed load. In

the composite stage, the bridge deck is active and connected to the girder with bond constraints. Finally, in the four-point bending stage, loading pins apply force to the deck in displacement-controlled loading. The ultimate load of this stage is the total live load that the section can withstand in addition to the dead load.

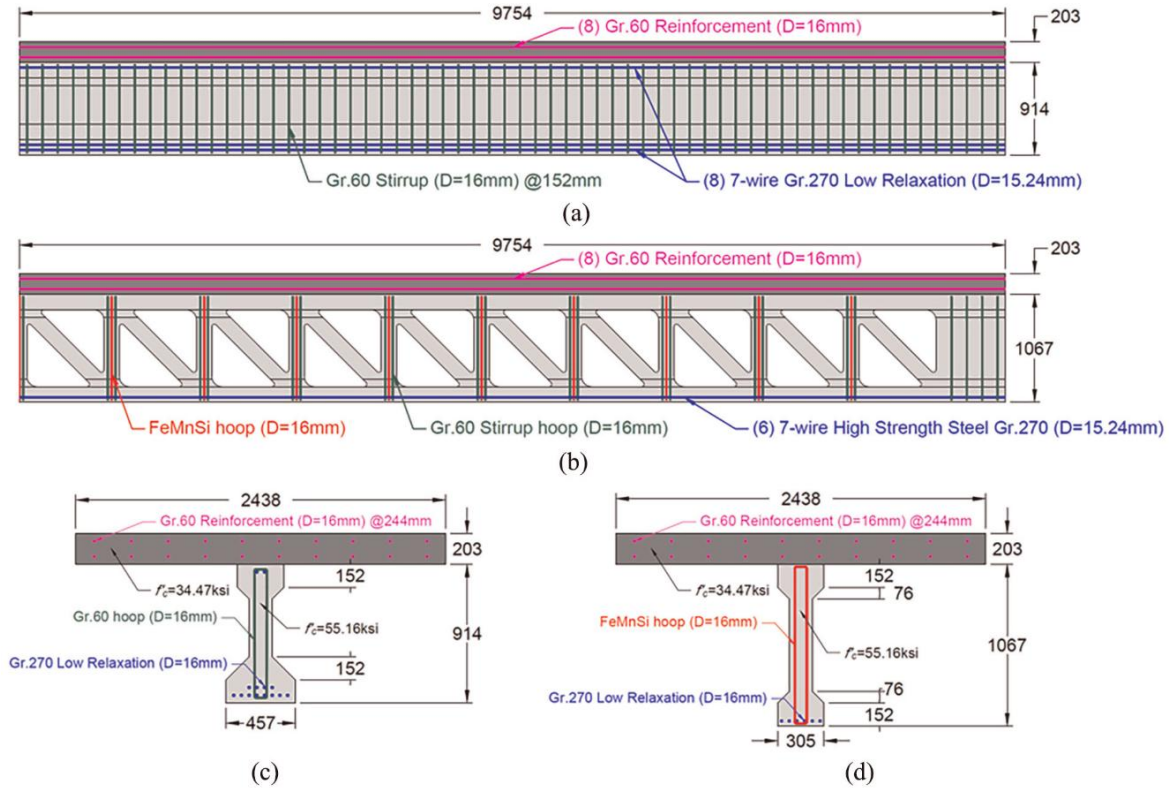

Fig. 5. Elevation of (a) AASHTO type II bridge and (b) concrete truss bridge; Cross-section of (c) AASHTO type II and (d) concrete truss.

The maximum and minimum principal stress contour plots from the ABAQUS analysis of the two bridges are shown in **Fig. 6**. **Fig. 6(a) and (b)** show the stresses for the reference bridge. **Fig. 6(c) and (d)** show the stresses for the concrete truss bridge with activated SMA. **Fig. 6(e) and (f)** show the stresses for the concrete truss bridge with unactivated SMA. The difference in the plots shows the effectiveness of activated SMA. When comparing the reference girder to the truss girder, the truss girder has higher stresses at the top and bottom of the section. This is due to the reduced moment of inertia caused by the voids in the web region.

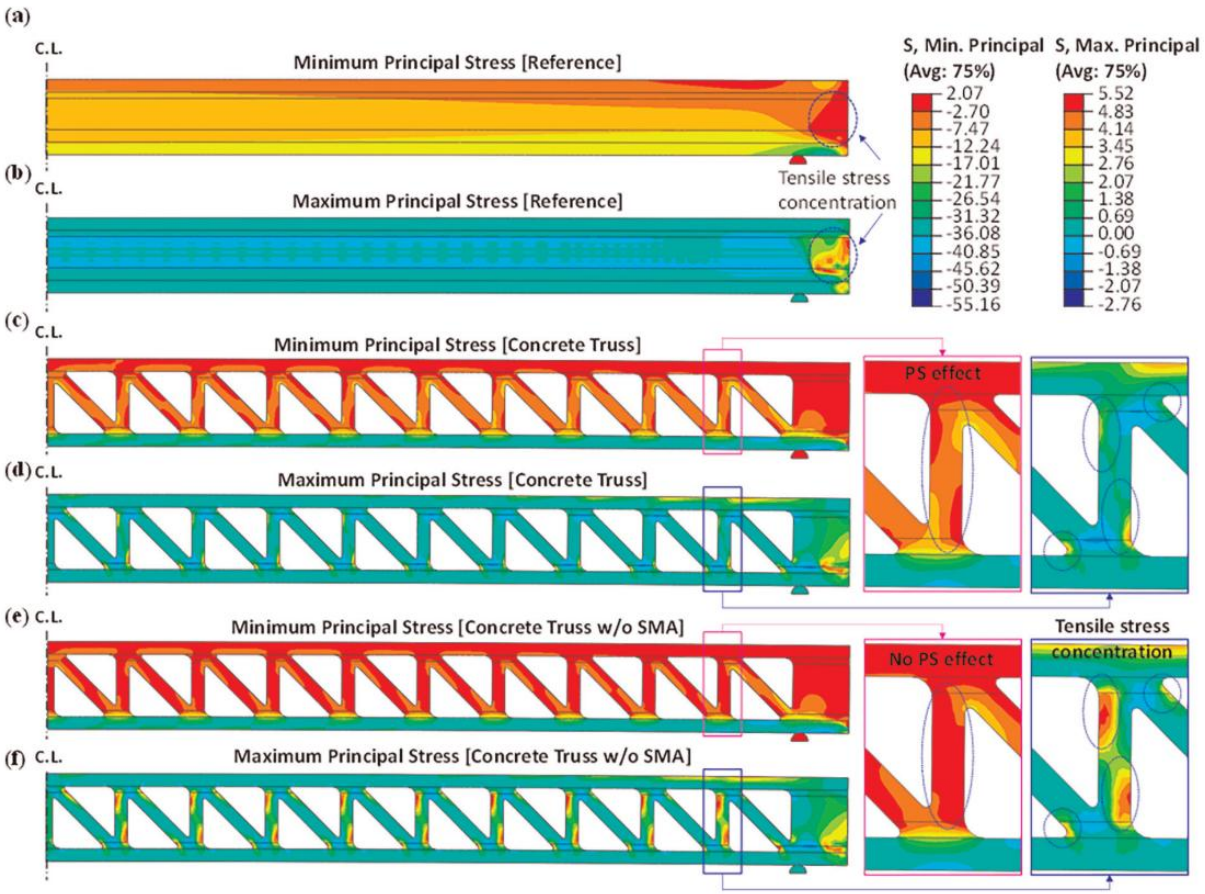

Fig. 6. Principal stress contour after applying prestress of reference bridge: (a) minimum principal stress, (b) maximum principal stress; concrete truss bridge, (c) minimum principal stress, (d) maximum principal stress; concrete truss bridge without activating vertical SMAs, (e) minimum principal stress, and (f) maximum principal stress.

The live load capacity and demand curves of the bridges are shown in **Fig. 7**. The dead loads differed between the two models, so only the additional load at the bending stage is shown. This additional load represents the capacity for live load. The figures show the distance from mid-span to the loading pin for each shear span case. The dashed lines represent the demand curves for bending moment and shear force in accordance with AASHTO strength I limit state live load. Both bridges exceed the limit state at all locations.

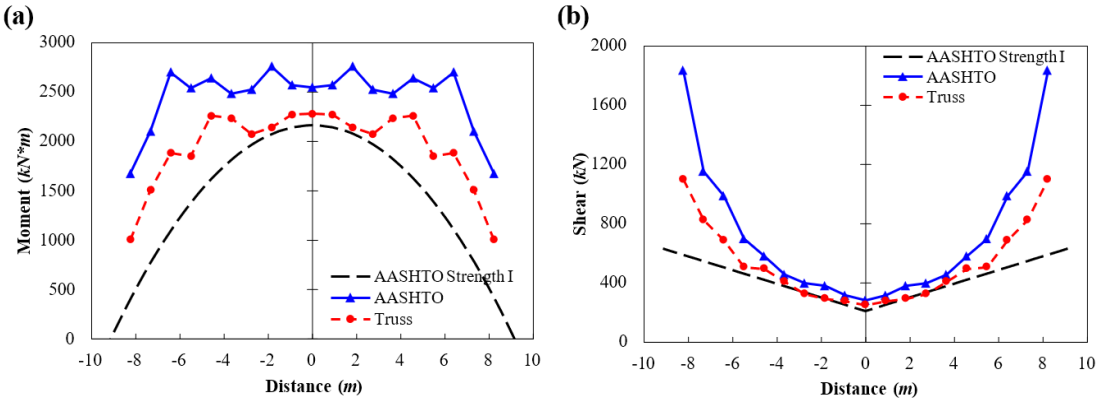

Fig. 7. Demand versus capacity curves of the bridges for (a) moment and (b) shear.

A reference bridge was developed to compare a conventional girder to an innovative concrete truss girder. The lower chord of the truss was prestressed using conventional HSS, while the vertical members were prestressed using SMAs. The bridges were modelled in ABAQUS, and both satisfied the AASHTO strength I limit state. The concrete truss reduces 37.8% of the concrete volume and 26.5% of the prestressing steel. The result is a 37.3% reduction in total weight when compared to the reference AASHTO type II girder. This confirmed that the use of truss geometry with SMA prestressing can improve the efficiency of concrete bridge girders.

4.2 Design of Concrete Truss Bridge Girders using Finite Element Method

This task focused on optimizing the girder design by conducting a comprehensive parametric study. The key design variables were truss length and depth, flange dimensions, web thickness, number and size of voids, and number and configuration of SMA reinforcement in the vertical members. The truss span ranged from 20 to 35 feet, and the depth ranged from 36 to 60 inches, as these were realistic limits for concrete girders. The aim was to optimize the truss to achieve a longer span than a conventional AASHTO girder while using less concrete.

Different truss configurations were analyzed and evaluated using the FEA software ABAQUS. The most optimal design was a 26-foot-long truss (**Fig. 8**), which represents a 30% increase in span length and a 25% reduction in concrete when compared to a conventional 20-foot AASHTO I-girder. This truss was then modified to investigate the efficiency of using SMA for prestressing (**Fig. 9**). The steel reinforcement in the vertical members is replaced with SMA to increase the load-bearing capacity of the truss and to delay crack initiation.

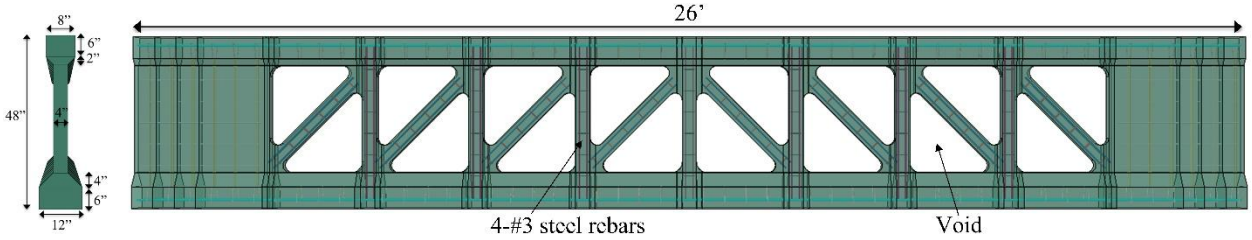

Fig. 8. Optimized truss system with steel reinforcement

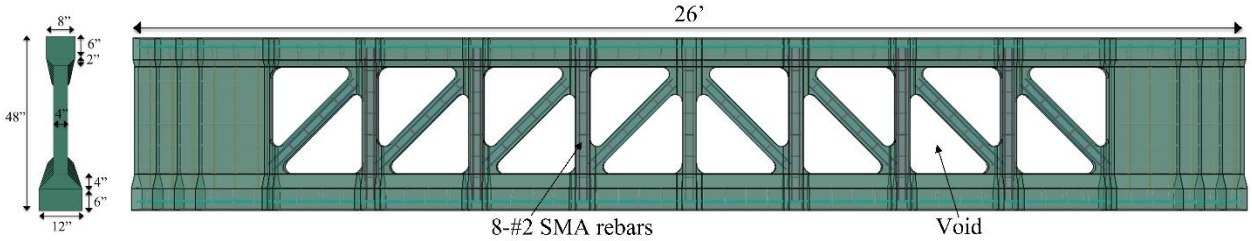

Fig. 9. Optimized truss system with SMA reinforcement

The FEA results confirmed that the cracking load of the truss increased by 46%. This confirms that a truss girder with SMA can reduce concrete usage while increasing the span length and still satisfying AASHTO LRFD design specifications.

4.3 Fabrication, Instrumentation, and Testing of UHPC and FRP Reinforced with SMA

This part of the study used three different concrete mix designs (**Table 1**) for potential application in bridge truss structures reinforced with SMAs. The first was a mortar mix design using cement,

sand, water, and a high-range water reducer (HRWR). The second was an FRC, containing similar materials but with 0.5-inch-long steel fibers replacing 1% of the sand by volume. The third mix design was a UHPC made from cement, sand, water, steel fibers, COR-TUF, a high-range water reducer (Visco 1000), a workability retaining admixture (Visco 2020), and the corrosion inhibitor (CNI). COR-TUF is a proprietary material created by the U.S. Army Corps of Engineers Engineer Research and Development Center for manufacturing UHPC (Roth et al., 2010; Williams et al., 2009). At 28 days, cubes with 2-inch long sides were tested, and the compressive strengths of the concrete, FRC, and UHPC were 8.3 ksi, 10.8 ksi, and 18 ksi, respectively.

Table 1. Concrete Mix Designs

	Cement (lb/ft^3)	Sand (lb/ft^3)	Water (lb/ft^3)	HRWR (lb/ft^3)	Steel Fiber (lb/ft^3)	COR-TUF (lb/ft^3)	Visco 1000 (lb/ft^3)	Visco 2020 (lb/ft^3)	CNI (lb/ft^3)
Concrete	45.3	91.0	14.0	0.7	0	0	0	0	0
FRC	45.3	90.0	14.0	0.7	5.0	0	0	0	0
UHPC	48.5	50.7	10.0	0	9.8	40.0	2.7	2.1	1.7

Aside from mix design, the other parameters were the presence of SMA, the heating method, and whether activation was before or only after cracking occurred. To study all these variables, thirteen specimens were fabricated. Four were conventional concrete, four were FRC, and five were UHPC. One specimen from each group contained no SMA to function as a reference specimen. One specimen in each group is heated before cracking to study the effects of prestressing. Two specimens are heated after cracking with either electricity or induction heating. The UHPC had one additional specimen to be used for studying induction heating for SMA prestressing.

These specimens were designed as flexural members, so the SMA is located near the bottom. The dimensions were 1.2 inches wide, 2 inches high, and 10 inches long (**Fig. 10**). The first step in fabricating the specimens was to prestrain and cut the SMA bars. The SMA extended outside the concrete at the ends to serve as a direct connection for heating with electricity. Copper crimp connectors were crimped along the length of the SMAs and spaced 1 inch apart. This arrangement prevented crimps from being near the midspan and influencing the crack behavior.

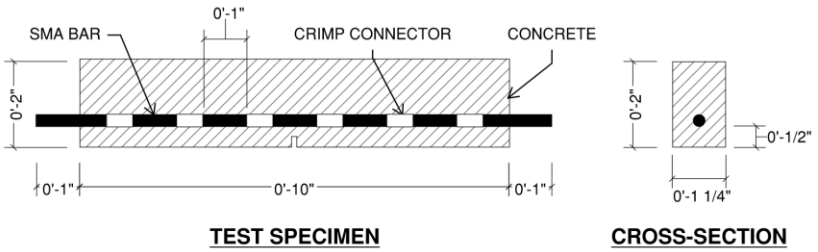

Fig. 10. Test specimen design

One thermocouple was secured to each SMA bar. These thermocouples are crucial for monitoring the SMA temperature during heating to ensure it reaches the activation temperature. Failure to reach the activation temperature will lead to incomplete activation of the SMA. On the other hand, excessively high temperatures can cause unnecessary stress in the surrounding concrete. Metal molds were modified to allow simultaneous casting of three specimens (**Fig. 11a**). Holes were drilled into foam blocks, which were then slipped over the SMAs. Wooden partitions are added as barriers, and a small groove is cut at the midpoint. Another piece of wood was

pressed into the grooves after pouring the concrete to form the notches for crack initiation (**Fig. 11b**). After a day, the specimens were demolded and placed in a humidity-controlled room. After curing, the specimens were removed and dried.

(a) (b)

Fig. 11. (a) Formwork with SMA inside, and (b) formwork after concrete was poured

One side of the specimen was painted white to facilitate the inspection for cracks (**Fig. 12**). A strain gauge was mounted on the opposite side of each specimen. They were centered above the notches and aligned with the SMAs. A crack mouth opening displacement (CMOD) gauge was also used for this study. This device has two metal prongs that attach to the sides of the notch to measure the change in the crack opening. The clamps cannot attach to the concrete directly, so metal blades are bonded with epoxy resin around the opening to serve as attachment points. A data acquisition system (DAQ) was used to collect readings from the instruments and transfer them to a laptop.

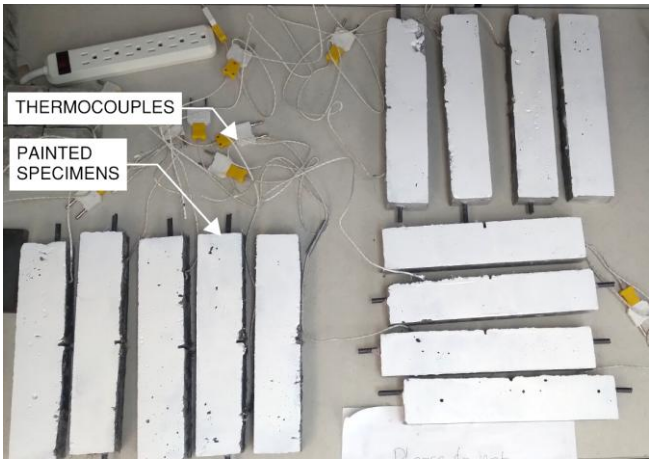

Fig. 12. Specimens after painting

Two different heating methods are used to find a safe and efficient heating method. The first method uses the electrical resistivity of the SMA to heat it. This is suitable for cases where SMAs are embedded in conventional concrete, as it is quick and requires minimal equipment. The power supply used in this study is a portable device with an output of 400 amps. As shown in **Fig. 13a**, two cables connect the power supply to the exposed ends of the SMA bars. The specimen is placed on a pair of concrete roller supports to eliminate friction and prevent heat transfer to the table. The second method uses induction heating. Pérez-Claros & Andrawes (2025) successfully used this method to heat SMAs embedded inside concrete. The induction heater used in this study (**Fig. 13b**) works by passing a current through a copper coil to generate magnetic fields. These magnetic fields induce eddy currents in any nearby metal, heating it up. The copper induction coil is also affected by these eddy currents, thus requiring a constantly circulating coolant inside it. The coil was custom-fabricated to match the dimensions of the test specimens. It is a “pancake” coil, with one coil loop nested within another.

(a) (b)

Fig. 13. Setup for heating using (a) electricity and (b) induction

A three-point bending setup was used to crack the specimens (**Fig. 14**). The specimen was placed within a 25 kip loading frame on metal supports. The supports contain cylindrical bearings that eliminate torsion of the specimen. A rounded metal blade was fixed to the actuator of the loading frame to load the specimen at its midspan.

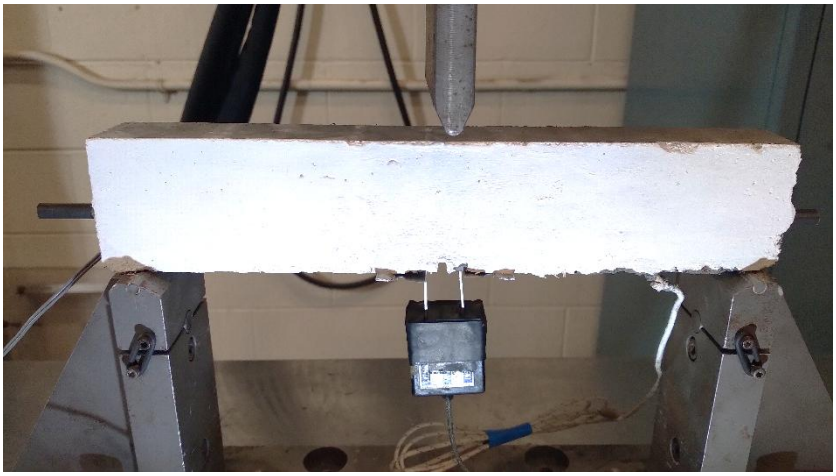

Fig. 14. Flexural loading test setup

To keep track of the specimens, each was assigned a three-letter identifier. The first letter indicated the mix design: “N” for mortar, “F” for FRC, and “U” for UHPC. The second letter indicated the heating method: “E” for electricity and “I” for induction. The third letter indicated when heating was applied: “B” for heating before loading and “A” for heating after loading. This is summarized in **Table 2**.

Table 2. Test Plan Matrix

Identifier	Mix Design	Reinforcement	Prestressing	Healing
NNN	Mortar	-	-	-
NEB	Mortar	SMA	Electricity	-
NIA	Mortar	SMA	-	Induction
NEA	Mortar	SMA	-	Electricity
FNN	FRC	-	-	-

FEB	FRC	SMA	Electricity	-
FIA	FRC	SMA	-	Induction
FEA	FRC	SMA	-	Electricity
UNN	UHPC	-	-	-
UIB	UHPC	SMA	Induction	-
UEB	UHPC	SMA	Electricity	-
UIA	UHPC	SMA	-	Induction
UEA	UHPC	SMA	-	Electricity

Cube specimens with side lengths of 2 inches were tested on the day of the experiment. The compressive strengths of mortar, fiber-reinforced concrete (FRC), and ultra-high performance concrete (UHPC) were 10.1 ksi, 12.3 ksi, and 21.8 ksi, respectively. The procedure in this study consisted of prestressing, loading, and healing. During the prestressing stage, NEB, FEB, UEB, and UIB specimens were heated, and the other nine specimens remained unheated. NEB, FEB, and UEB specimens were electrically heated until the SMA exceeded 392 °F, and then slowly cooled to the initial temperature. The UIB specimen was heated using the induction machine until the temperature of the SMA exceeded 392 °F, and then slowly cooled to the initial temperature. During the loading phase, all specimens were subjected to three-point bending to induce cracking. The loading was displacement-controlled with a loading rate of 0.01 inch/min. The force, displacement, and crack opening displacement (CMOD) values were recorded during loading and unloading of each specimen. The stopping point for the mortar specimens was a CMOD reading of 0.012 inch because this value conforms to the permissible crack width recommended by American Concrete Institute (ACI) Committee 224 for moist air exposure conditions (ACI, 2001). Loading of NEB and NEA was stopped when the CMOD reached 0.012 inch. Loading of NIA was stopped at a larger CMOD value of 0.025 inch due to a delay during the operation of the load frame. The stopping criteria differed for the FRC and UHPC specimens because the steel fibers resisted crack propagation, and a CMOD value of 0.012 inch was insufficient. The criterion for stopping was based on the load cell reading. The FRC and UHPC specimens were loaded until their capacity decreased by 5%–10% of their respective overall maximum capacity. During the healing phase, the SMA was activated to trigger crack closure. The setup for heating was the same as during the prestressing phase.

5.1.1 Effect of SMA Prestressing on Delaying Cracks

The first objective of this study was to evaluate the effect of SMA activation on delaying crack formation. To this end, the SMAs in specimens NEB, FEB, UEB, and UIB were activated before loading to generate prestressing. The strain gauges at the midspan of each specimen measured the longitudinal strain on the surface under the prestressing forces. **Fig. 15a, b, c,** and **d** show the compressive strain recorded during the heating and cooling process of the SMA in specimens NEB, FEB, UEB, and UIB, respectively. All specimens exhibited fluctuations between compressive and tensile strains in the initial heating phase. This was due to the conflict between tensile strains from SMA thermal expansion and compressive strains from SMA shape recovery effect. The difference in initial strain response between UEB and UIB was most pronounced in this regard. UIB had a higher initial tensile strain due to the induction heating affecting the metal fibers in the UHPC and increasing the effect of thermal expansion. In all four specimens, the strains became compressive after the SMA reached its activation temperature of 392 °F. The

permanent compressive strains of NEB, FEB, UEB and UIB were 55 με, 27 με, 59 με and 1049 με, respectively.

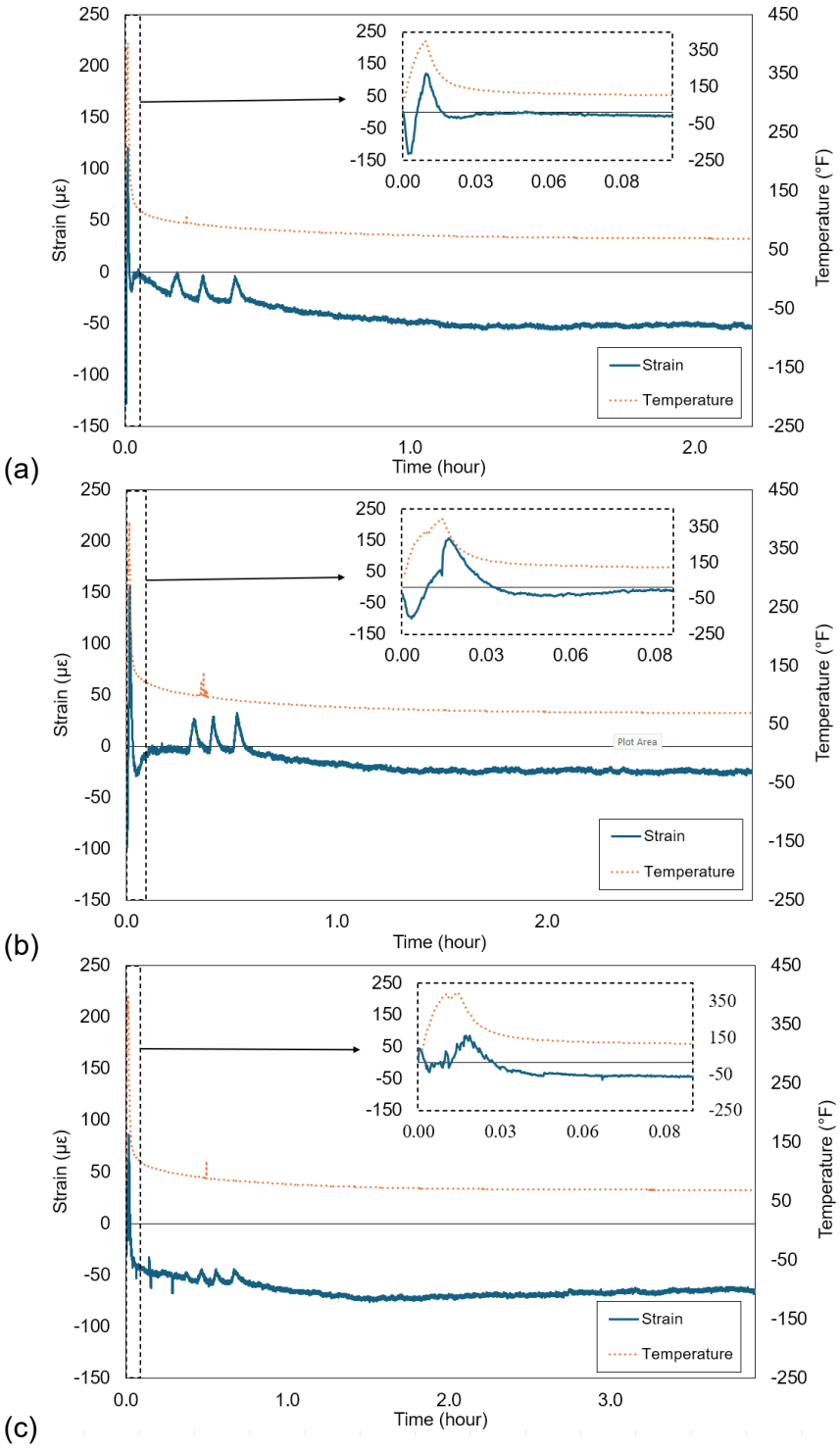

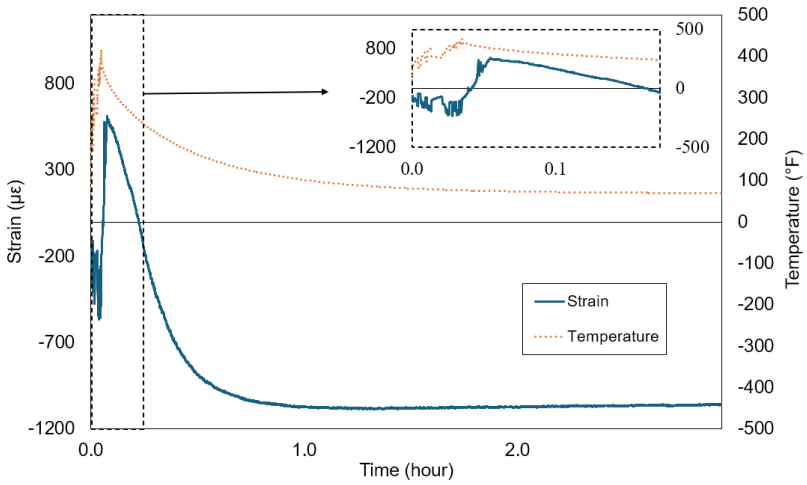

(d)

Fig. 15. Concrete compressive strain and SMA temperature over time for (a) NEB, (b) FEB, (c) UEB, and (d) UIB.

During heating, NEB developed longitudinal splitting cracks (**Fig. 16a**), indicating that prestressing was achieved. The FEB and UEB specimens did not exhibit splitting cracks because of their higher crack resistance. During heating, the UIB specimen experienced explosive spalling on the side near the induction coil. As shown in **Fig. 16b**, a portion of the cover spalled off, leaving a dent. This may have contributed to UIB having the highest compressive strain out of the four prestressed specimens. The force generated from the explosive spalling may have left permanent deformations in the specimen. This deformation, in turn, may have amplified the strain gauge readings in UIB.

(a) (b)

Fig. 16. (a) Crack in NEB and (b) spalling in UIB.

The results from NEB, FEB, UEB, and UIB show that both electricity and induction can heat the SMAs to their activation temperature. Thus, the choice depends on the type of concrete the SMA is embedded in. For UHPC, heating with electricity is safer than induction heating because it does not cause explosive spalling. However, with some modifications, induction heating may become suitable for UHPC. The activation temperature of SMAs varies depending on the SMA composition. Using SMAs with lower activation temperatures can prevent spalling. The mix design of UHPC can be improved. Researchers have demonstrated that adding polypropylene (PP) fibers to UHPC can prevent spalling (Hernández-Figueirido et al., 2024; J. Yang et al., 2019). Changes in curing regimes can also improve the UHPC spalling resistance (Qin et al., 2021).

To quantify the effect of SMA on delaying cracks, a comparison was needed between prestressed and unstressed specimens. To this end, all specimens were subjected to bending

loads to induce cracking. A common degree of damage was required to assess the performance across all the different specimens. A CMOD value of 0.012 inch was chosen to match the allowable crack width recommended by the ACI 224 committee. **Fig. 17** summarizes the load reached by each specimen while at a CMOD reading of 0.012 inch. The only exception was the NNN specimen, whose CMOD value was unavailable. This is because the CMOD gauge could not capture its sudden brittle failure. In the NIA and NEA specimens, no sudden failure occurred because the SMA acted as passive (unactivated) reinforcement. The NEB specimen showed further improved performance owing to the SMA prestressing. The average load for NIA and NEA was 271 lb, while the load for NEB was 436 lb, representing a 61% increase in capacity. The FRC specimens showed a similar trend. The unreinforced FNN specimen reached 227 lb. The specimens reinforced with passive SMA (FIA and FEA) had an average load of 776 lb, which is a 242% increase compared to FNN. Activation of the SMA in FEB increased its capacity to 912 lb, which is a 302% increase compared to FNN and an 18% increase compared to the average of FIA and FEA. In both FRC and mortar cases, the force required for the prestressed specimens to reach the same CMOD value was significantly greater. In other words, the prestressing of the SMA successfully delayed crack initiation because the prestressed specimens required greater force to achieve the same degree of cracking when compared to specimens without prestressing.

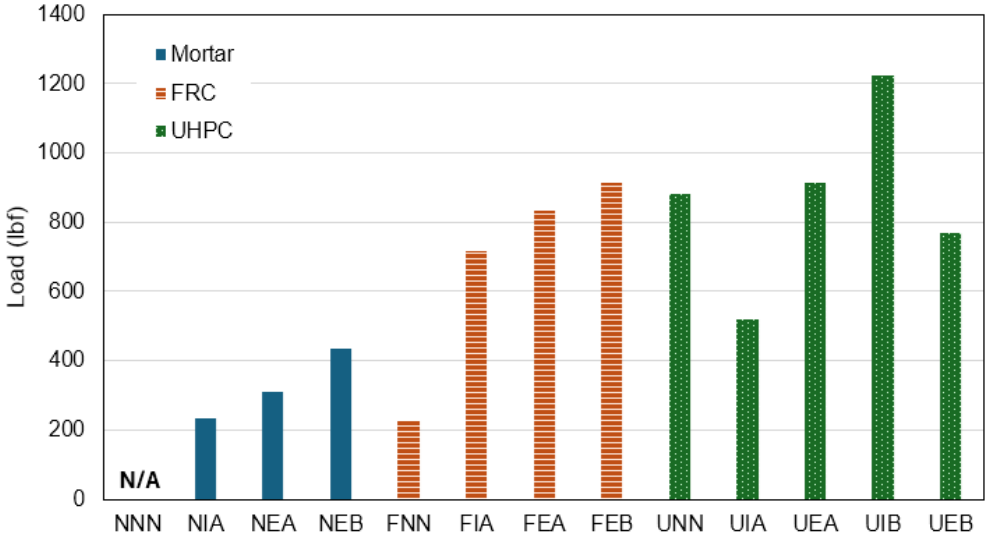

Fig. 17. Force corresponding to CMOD of 0.012 inch.

The effect of SMA incorporation in UHPC is not as clear as it was for mortar and FRC. There is a wider deviation in the measured loads among the five UHPC specimens. The UNN specimen reached a load of 881 lb without needing any SMA. The two specimens with passive SMA (UIA and UEA) had an average load of 716 lb, representing a 19% decrease in capacity compared to UNN. This decrease may be due to the anisotropy of UHPC caused by fiber orientation effects. Experimental evidence from Maya Duque & Graybeal (2017) suggests that the flow pattern during casting affects fiber orientation, which in turn affects the tensile mechanical properties of UHPC. The presence of SMA reinforcement during casting altered the flow pattern because the UHPC needed to flow around the SMA. This may have caused less desirable fiber orientations, leading to lower load capacities for UEA and UIA compared to UNN. Since UIB and UEB had the same internal reinforcement, they would also have lowered capacities relative to UNN. However, the prestressing of UIB was able to overcome this decrease. UIB had the highest capacity among all specimens, reaching 1225 lb. Compared with UNN, its capacity was increased by 39%, which shows the successful implementation of SMA in delaying crack initiation. UEB, on the other hand, had less prestressing force than UEB. This is evidenced by the strain in UEB

being almost 18 times less than UIB. Therefore, UEB performed worse than UIB. Another factor that affected UEB and UIB is the heating of UHPC in general. Since the only specimens that were exposed to high temperatures were also the ones that were prestressed, any negative effects of heating could not be identified. Exposure of the UHPC to high temperature could have produced internal stresses that weakened the specimen without leaving external signs.

5.1.2 Effect of SMA Activation on Crack Closure

Specimens NEA, FEA, and UEA were healed using electricity, and the CMOD gauge was used to measure the change in crack widths. Specimens NIA, FIA, and UIA were healed using induction heating. The CMOD gauge could not be used with the induction heater because the electromagnetic waves can damage the instrument. Therefore, a ruler was used to measure the crack width before and after heating. The ruler's accuracy was lower than that of the CMOD gauge. Thus, the samples were evaluated in two groups based on the heating method to eliminate the influence of instrumentation differences.

Fig. 18 shows the results of the specimens healed using the induction heater. Induction heating activated the SMAs and reduced the crack width of all three types of concrete. During heating, the NIA specimen performed well, and its crack width reduced by 80%. The FIA specimen responded well, with a crack width reduction of 90%. The UIA specimen experienced explosive spalling under induction heating, which emphasized the previous conclusion that induction heating of SMA in UHPC requires special attention. The area near the notch was undamaged, so the crack could still be measured with a ruler. Its crack width was reduced by 84%.

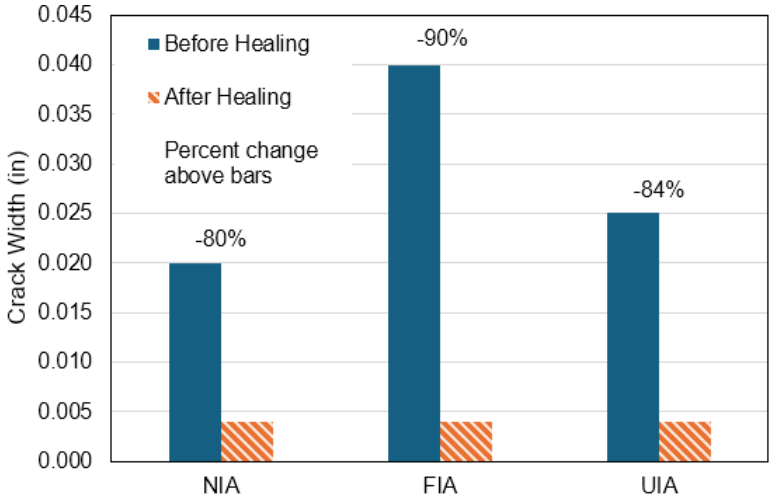

Fig. 18. Crack closure when heating with induction.

Fig. 19 shows the results for the specimens healed using electricity. It can be seen that SMA activation induced crack closure in all three types of concrete. The NEA specimen had the highest crack width reduction of 74%. Visual inspection of the NEA specimen revealed longitudinal splitting cracks, indicating that prestressing had occurred. The FEA and UEA specimens had lower crack width reductions because the damage in FEA and UEA from the initial test was much greater than that of NEA. The FEA specimen had the largest crack and showed a reduction of 65%. The UEA specimen had the lowest crack width reduction of 60%.

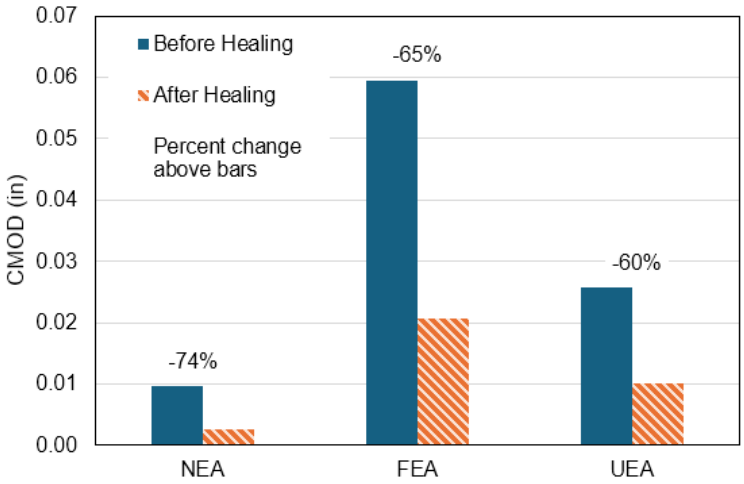

Fig. 19. Crack closure when heating with electricity.

The study showed that SMA bars can transfer prestress to different types of concrete, including mortar, fiber-reinforced concrete (FRC), and ultra-high performance concrete (UHPC). This prestress improves durability by delaying cracking. Alternatively, the SMA bars can be used to heal the different types of concrete. Activation of the SMA reduced crack widths in the mortar, FRC, and UHPC specimens by up to 80%, 90%, and 84%, respectively.

4.4 Fabrication, Instrumentation, and Testing of Flexural Specimen

This task focused on the use of SMA bars to heal flexural specimens. The SMAs were prestrained and embedded as reinforcement in a concrete beam. The ends of the SMAs were bent into hooks to provide anchorage. A CMOD gauge was used to track the opening of the crack. The specimen was first cracked in a three-point bending setup. The SMAs were activated to trigger crack closure. The specimen was then reloaded to open the crack again. The SMAs were activated a second time. Finally, the specimen was loaded until failure.

A small-scale beam test specimen was fabricated. Two 0.08-inch-diameter SMA wires were embedded into a concrete beam near the bottom (**Fig. 20a**). These two SMA wires were pre-strained to 6% and bent into 90-degree hooks at both ends. Metal plates were wrapped around the hooks for additional reinforcement. A thermocouple was attached to the SMAs prior to casting. A crack opening displacement (COD) gauge and a strain gauge were installed on the specimen to monitor the crack propagation (**Fig. 20b**). One face was painted white to improve the visibility of the cracks.

(a)

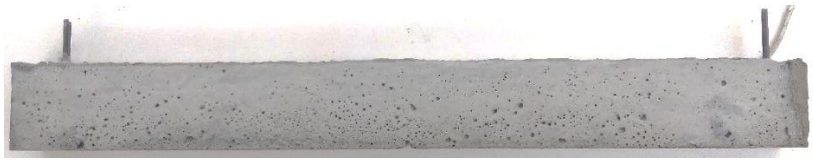

(b)

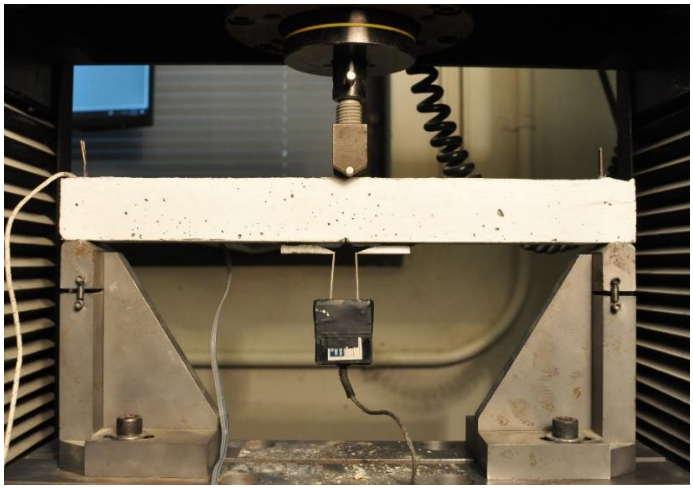

Fig. 20. (a) Test specimen after curing and (b) during flexural test

A three-point bending test was performed on the beam until the CMOD read 0.011 inch (**Fig. 21a**). The beam was unloaded, and the SMA was connected to the power supply. Current was passed through the two SMA wires, triggering the shape memory effect and closing the crack (**Fig. 21b**).

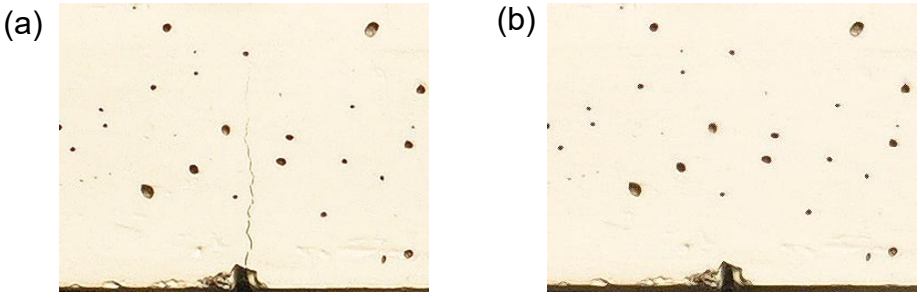

Fig. 21. (a) Crack during loading and (b) crack after activation

The beam was reloaded again, but this time until the CMOD reached 0.019 inch (**Fig. 22a**). The SMA was heated a second time (**Fig. 22b**) to explore the repeatability of the procedure.

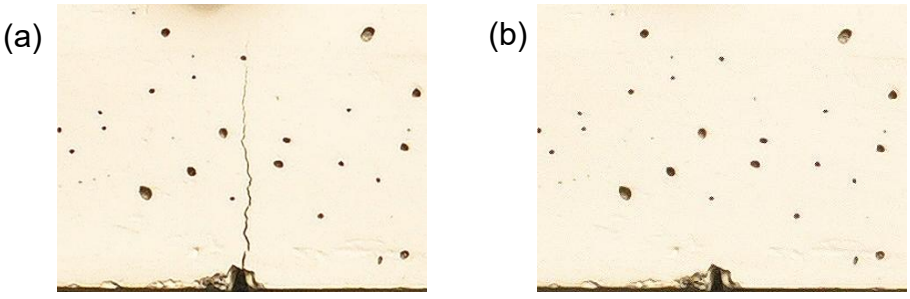

Fig. 22. (a) Crack during re-loading and (b) crack after re-activation

The activation of the SMA bars healed the specimen by closing cracks as wide as 0.02 inch. The activation also improved the structural performance in the beam, thus validating the use of SMA bars to improve the durability of concrete structures. Furthermore, the healing can be repeated multiple times, although its effectiveness is affected by the size of the crack.

4.5 Fabrication, Instrumentation, and Testing of Tensile Specimen

This task focused on using SMA bars to prestress and heal a tensile specimen representing truss members subjected to tension. The SMAs were prestrained and placed inside a specimen representing a small-scale tensile member from a concrete truss. The SMAs were activated prior to loading to prestress the member, and strain gauges were used to measure the prestressing force. The specimen was then loaded under uniaxial tension until cracking developed. The SMA bars were then activated once more to trigger crack closure and assess the effect of SMAs for healing tensile cracks.

Four prestrained SMA bars with diameters of 0.25 inches were embedded in a concrete specimen. The bars were sequentially heated with electricity to trigger their shape memory effect. Strain gauges were attached to the center of the specimen (**Fig. 23**). The specimen was then loaded to cracking, and then reheated to heal the damage.

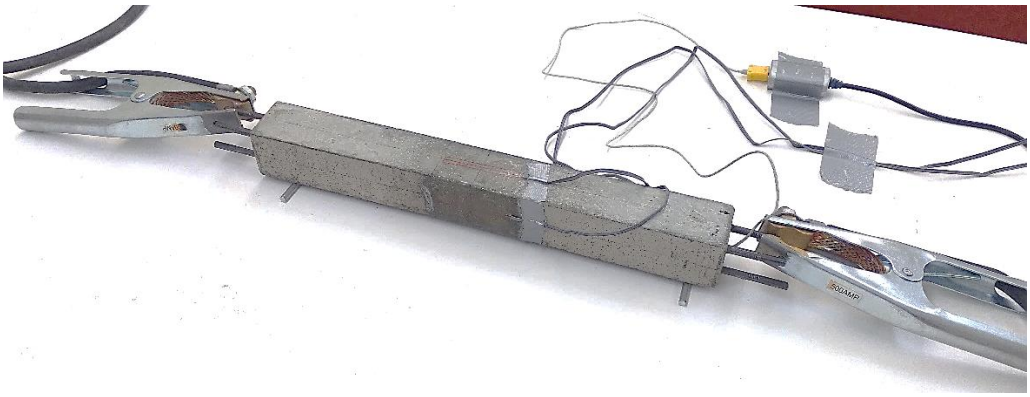

Fig. 23. Activation of tensile specimen

Four aluminum plates were bonded to the specimen using epoxy. These were then connected with ball joints to the load frame. The specimen was loaded axially under pure tension. The test concluded when a 0.02-inch-wide crack developed near the center of the specimen (**Fig. 24a and b**). After unloading, the SMAs were heated again to activate the shape memory effect. This caused the crack to close completely (**Fig. 24c**), demonstrating that SMAs can be used to repair concrete tensile damage.

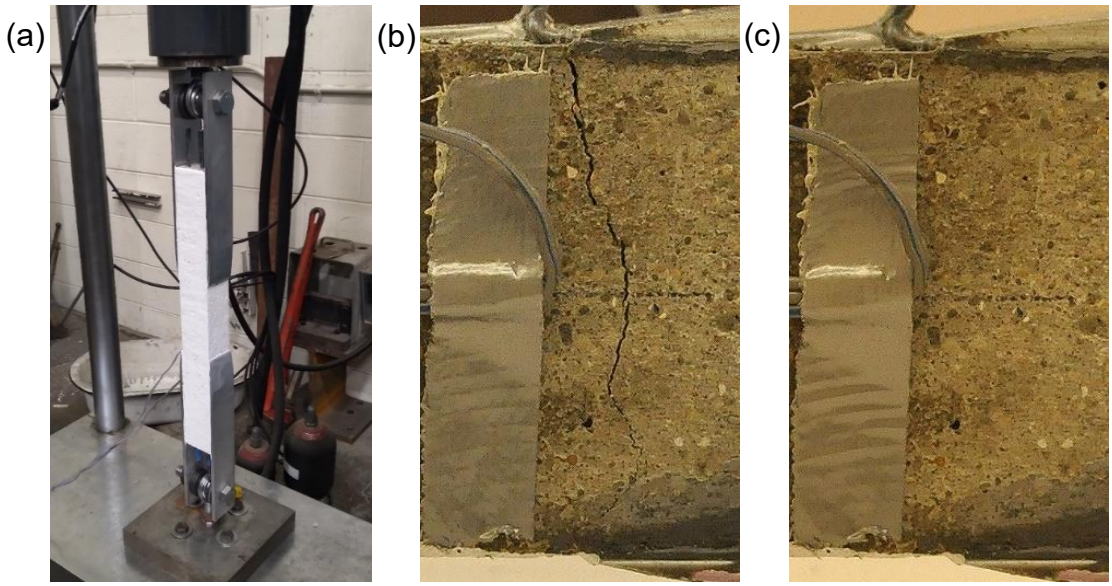

Fig. 24. (a) Test setup, (b) crack before healing, and (c) crack after healing

Activation of the SMA bars successfully prestressed the concrete tensile test specimen. This validated the use of SMAs to improve the durability of concrete tensile members by delaying crack onset. The activation of the SMA bars after loading closed cracks as wide as 0.02 inches validates the use of SMA bars for improving the durability of trusses reinforced with SMA bars.

4.6 Fabrication, Instrumentation, and Testing of Large-Scale Truss Girder

The final task of the project is the fabrication and testing of a large-scale truss girder. The design is based on the results from the numerical studies in Task 2. The dimensions were adjusted to simplify construction and transportation, with the most notable change being the reduction in length. It is a Howe truss with four bays, which corresponds to three vertical members in the truss. This allows for two verticals to be studied simultaneously. The truss design was developed by introducing voids into an AASHTO Type II girder. Eight triangular voids were added to the web (**Fig. 25**), transforming the girder's structural behavior from a beam to a truss composed of compression and tension members. The girder height was also increased to counteract the loss in stiffness. The top and bottom widths were reduced to compensate for the reduction in reinforcement. One vertical was reinforced with steel, and the other was reinforced with SMAs. The side with SMAs was activated with an induction heating machine to produce prestressing forces and delay the onset of cracking. The truss was then loaded in three-point bending. It was instrumented with DIC and strain gauges to capture its behavior during prestressing and loading. These measurements were used to quantify the benefits of SMAs for concrete truss systems.

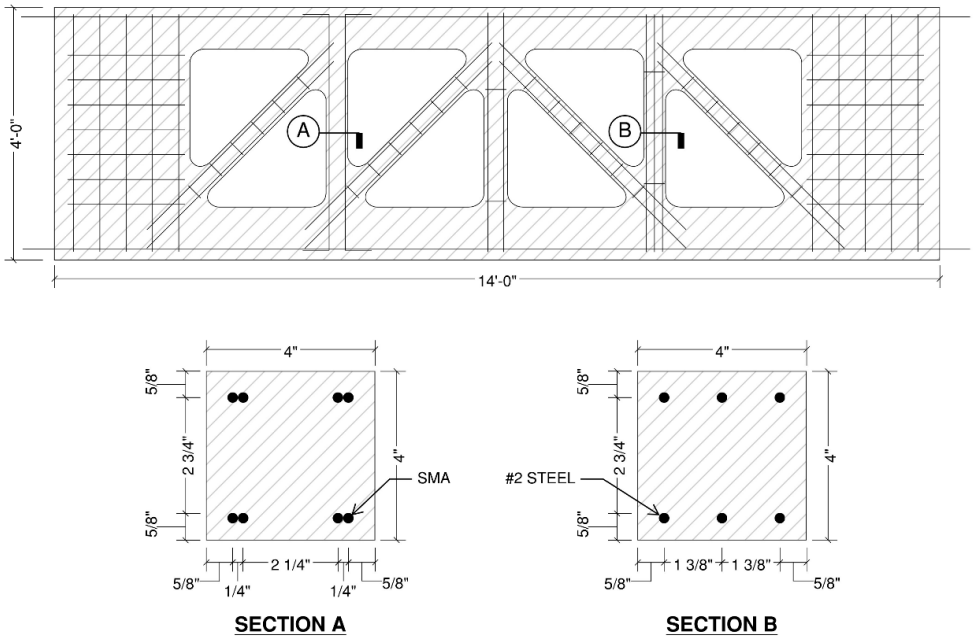

Fig. 25. Precast truss reinforcement layout

Finite element analysis was used to determine the locations of maximum tensile stress and cracking. The girder was simply supported with a concentrated load applied at midspan. After iterative analysis, the model was modified to add optimal amounts of steel reinforcement and SMAs in areas prone to tensile damage. The outer vertical members experienced the highest tensile stress and are ideal locations to test SMA prestressing. However, only one member was reinforced with SMAs. It used eight 0.25” diameter SMA bars, while the other vertical used six #2 steel bars. This asymmetric design allowed a prestressed and an un-prestressed member to be studied simultaneously, eliminating the need to construct a second truss. Wood was used for the sides of the formwork. Foam boards were trimmed, stacked, and glued to the walls to form the outer profile. Foam triangles were cut and glued to the wall to create the voids.

Eight 0.25” diameter SMA bars were pre-strained for the vertical. Copper crimps were added along the middle of the bars, and the ends were bent into 90-degree hooks. Thermocouples were attached to one of the SMA bars. Steel rebars were cut, bent, and tied to form the rest of the reinforcement. The joints of the walls were sealed with a caulking compound. Wooden braces were added along the wall to provide out-of-plane support. Then, concrete was poured into the form, and vibrators were used to remove air bubbles. After curing and demolding, any voids were filled with high-strength grout. The specimen was painted white to aid in visual detection of cracks (**Fig. 26**). A speckle pattern was added to both verticals for use with DIC, and strain gauges were installed on the surface near critical regions.

Fig. 26. Cured and painted concrete truss

Fig. 27. Electromagnetic induction heating of the concrete vertical member

The prestressing stage required the use of the induction heater to heat the embedded SMAs past their transformation temperature. The bars were heated in increments using an induction heater (**Fig. 27**), and the thermocouples inside were used to determine the heating duration. The specimen was then allowed to fully cool to the starting temperature, and permanent compressive strains were measured by the strain gauges. The three strain gauges near the middle of the vertical had an average compressive strain of 301 με. The concrete compressive strength at the time of activation was 876 psi. By using **Equation 1** from AASHTO, this is converted to a modulus of elasticity of 1703 ksi. This, in turn, allows the strain to be equated to a prestress of 513 psi in the concrete.

$$E = 1820\sqrt{f_c'} \tag{1}$$

The specimen was then moved into a three-point bending test setup. An actuator delivered a concentrated load at the midspan of the truss, and a load cell between the actuator and truss measured the force applied. Two lights and two cameras were used for photographing the verticals for DIC measurements. Additionally, two string potentiometers were attached to the truss to track the vertical displacements. A DAQ on the side recorded the measurements from the load

cell, string potentiometers, and strain gauges. The specimen was slowly loaded, and the progress of cracking was monitored with the instrumentation and by visual inspection. The force in the load cell when the cracks first formed near the joints of the member without SMA was around 5 kip. On the other hand, cracks near the joints of the member prestressed with SMAs started around 35 kip. The difference between the members is visualized using **Fig. 28,** and the load for the member with SMA is 600% higher. More notable were the cracks that developed in the center-most region of the member without SMA. These cracks were away from the joints and, therefore, were due primarily to tension forces and not rotation at the joints. The DIC software colors the areas of highest vertical tensile strains in red, so the bands of red in **Fig. 28** are signs of cracking. There are no red bands on the side with prestressing, even at the peak load of 40 kip. Thus, the DIC results showed that the member reinforced with only conventional steel cracked before the member with SMA prestressing.

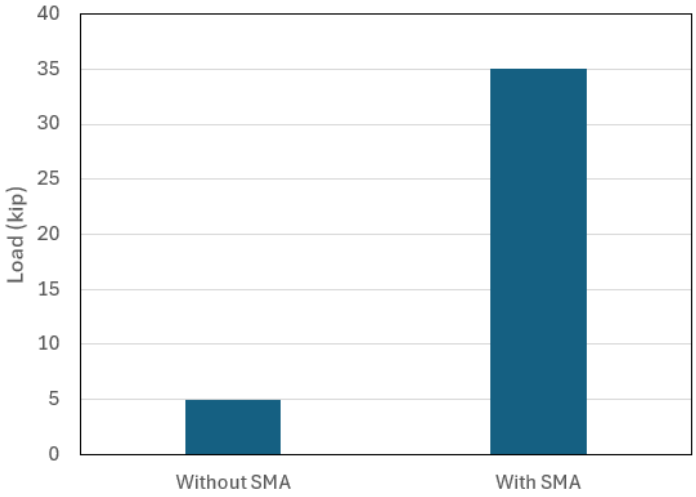

Fig. 28. Load when cracking near joints occurred

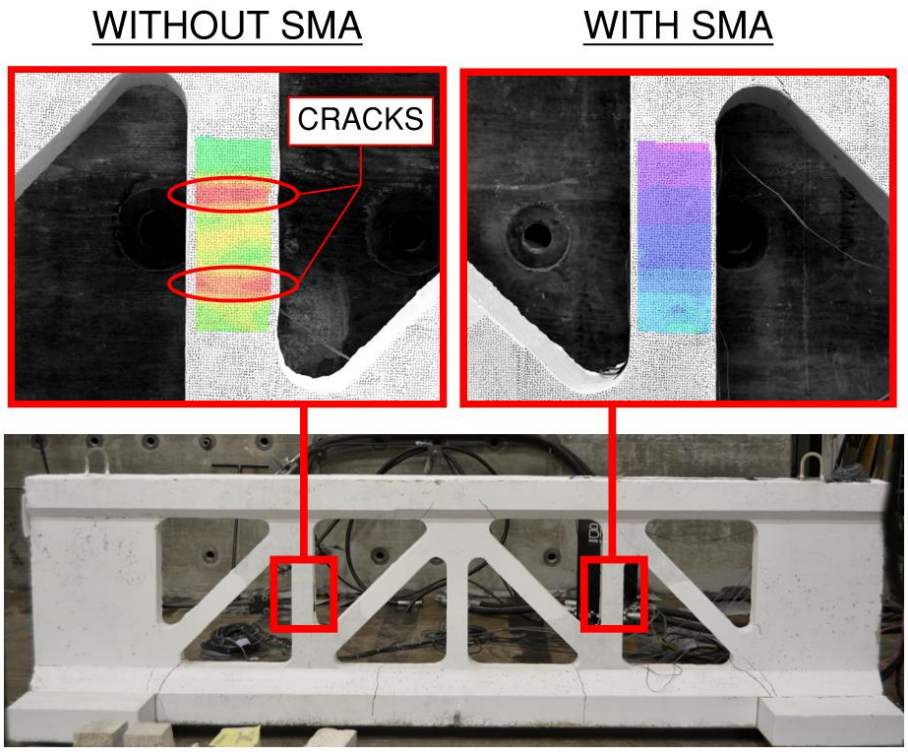

Fig. 29. DIC corresponding to a load of 40 kip

This part of the study experimentally validated prestressing with SMAs at a large scale. During the development of prestressing forces, no splitting cracks occurred in the member. This is a notable difference between the test results of the isolated member and a full system. The truss had additional material and rigidity at the ends of the prestressed member, thus preventing the splitting cracks. This showed that splitting cracks would not be an issue in practice. The flexural test validated the effects of prestressing in a truss system and opened up new possibilities in the construction of complex concrete geometries.

5. Practical application/impact on transportation infrastructure

Concrete truss systems have already been used for bridges in countries outside of the U.S., which proves their feasibility and practicality. The quickest way to implement this technology in the U.S. will be to modify existing metal forms for precast concrete. Pieces can be added inside the forms to form the voids, in a manner similar to how it was done in this research. Alternatively, these truss designs can be produced using a 3D-concrete printer to eliminate the issue of formwork. This will be an interesting area for potential future research.

The SMA prestressing and healing methods demonstrated in this research would be ideal for the aforementioned truss-based concrete structures. It can also be applied anywhere where prestressing is beneficial, such as beams and slabs. Moreover, this research showed that SMA prestressing and healing are not limited to conventional concrete and can be incorporated into UHPC components.

6. References

AASHTO. (2024). *AASHTO LRFD Bridge Design Specifications*.

American Concrete Institute. (2001). Control of Cracking in Concrete Structures. In *ACI 224R-01*. Farmington Hills, Michigan.

American Concrete Institute. (2007). Causes, evaluation, and repair of cracks in concrete structures. In *ACI 224.1R-07* (p. 22). Farmington Hills, Michigan.
American Concrete Institute. (2008). Use of epoxy compounds in concrete. In *ACI 503R-93*. Farmington Hills, Michigan.
Amir, O., & Shakour, E. (2018). Simultaneous shape and topology optimization of prestressed concrete beams. *Structural and Multidisciplinary Optimization*, *57*(5), 1831–1843. https://doi.org/10.1007/s00158-017-1855-5
Andrawes, B., Colombani, I., Mirdad, M. A. H., & Chen, A. (2024). *Load Rating of Reinforced Concrete Slab Bridges Using Field Testing*. https://doi.org/10.36501/0197-9191/24-025
Andrawes, B., Shin, M., & Wierschem, N. (2009). Active Confinement of Reinforced Concrete Bridge Columns Using Shape Memory Alloys. *Journal of Bridge Engineering*, 81–89. https://doi.org/10.1061/ASCEBE.1943-5592.0000038
Benaim, R. (2008). *The design of prestressed concrete bridges: concepts and principles*. www.eBookstore.tandf.co.uk.
Benjamin Graybeal. (2009, January). UHPC Making Strides. *Public Roads*, *72*, 17–21.
Chen, H.-J., Yu, Y.-L., & Tang, C.-W. (2020). Mechanical properties of ultra-high performance concrete before and after exposure to high temperatures. *Materials*, *13*(3). https://doi.org/10.3390/ma13030770
Choi, E., Nam, T.-H., Chung, Y.-S., Kim, Y.-W., & Lee, S.-Y. (2012). Behavior of NiTiNb SMA wires under recovery stress or prestressing. *Nanoscale Research Letters*. http://www.nanoscalereslett.com/content/7/1/66
Dassault Systèmes Simulia Corp. (2011). *ABAQUS 6.11*. Providence, RI.
Dommer, K., & Andrawes, B. (2012). Thermomechanical Characterization of NiTiNb Shape Memory Alloy for Concrete Active Confinement Applications. *Journal of Materials in Civil Engineering*, *24*(10), 1274–1282. https://doi.org/10.1061/(asce)mt.1943-5533.0000495
Fong, M., Chan, S. L., & Uy, B. (2011). Advanced design for trusses of steel and concrete-filled tubular sections. *Engineering Structures*, *33*(12), 3162–3171. https://doi.org/10.1016/j.engstruct.2011.08.002
Gallardo Fuentes, J. M., Gümpel, P., & Strittmatter, J. (2002). Phase change behavior of nitinol shape memory alloys. *Advanced Engineering Materials*, *4*(7), 437–452. https://doi.org/10.1002/1527-2648(20020717)4:7<437::AID-ADEM437>3.0.CO;2-8
Graybeal, B. A., & El-Helou, R. (2023). *FHWA-HRT-23-077: Structural Design with Ultra-High Performance Concrete*. https://www.ntis.gov
Griffin, S., Askarinejad, H., & Farrant, B. (2017). Evaluation of epoxy injection method for concrete crack repair. *International Journal of Structural and Civil Engineering Research*, 177–181. https://doi.org/10.18178/ijscer.6.3.177-181
Gunasekaran, D., Khan, A., & Andrawes, B. (2025). Innovative Repair of Transversely Cracked PPC Bridge Deck Girder using Precast Prestressing Plates with Shape Memory Alloys. *International Journal of Bridge Engineering, Management and Research*, *2*(3). https://doi.org/10.70465/ber.v2i3.39
Haber, Z. B., Foden, A., McDonagh, M., Ocel, J. M., Zmetra, K., & Graybeal, B. A. (2022). Design and Construction of UHPC-Based Bridge Preservation and Repair Solutions. In *FHWA-HRT-22-065*. https://doi.org/10.21949/1521867
Hernández-Figueirido, D., Reig, L., Melchor-Eixea, A., Roig-Flores, M., Albero, V., Piquer, A., & Pitarch, A. M. (2024). Spalling phenomenon and fire resistance of ultrahigh-performance concrete. *Construction and Building Materials*, *443*. https://doi.org/10.1016/j.conbuildmat.2024.137695
James, J. G. (1980). The evolution of iron bridge trusses to 1850. *Transactions of the Newcomen Society*, *52*(1), 67–102. https://doi.org/10.1179/tns.1980.005
Kim, T. K., & Park, J. S. (2021). Performance evaluation of concrete structures using crack repair methods. *Sustainability (Switzerland)*, *13*(6). https://doi.org/10.3390/su13063217

Lagoudas, D. C. . (2008). *Shape memory alloys*. Springer.
Lopez-Calvo, H. Z., Montes-García, P., Jiménez-Quero, V. G., Gómez-Barranco, H., Bremner, T. W., & Thomas, M. D. A. (2018). Influence of crack width, cover depth and concrete quality on corrosion of steel in HPC containing corrosion inhibiting admixtures and fly ash. *Cement and Concrete Composites*, *88*, 200–210. https://doi.org/10.1016/j.cemconcomp.2018.01.016
Maya Duque, L. F., & Graybeal, B. (2017). Fiber orientation distribution and tensile mechanical response in UHPFRC. *Materials and Structures*, *50*(1). https://doi.org/10.1617/s11527-016-0914-5
Menn, C. (2012). *Prestressed Concrete Bridges*. Birkhäuser.
Menna, C., & Esposito, L. (2022). *Flexural Behaviour of Steel-Reinforced Topology-Optimised Beams Fabricated by 3D Concrete Printing* (pp. 404–410). https://doi.org/10.1007/978-3-031-06116-5_60
Otieno, M. B., Alexander, M. G., & Beushausen, H. D. (2010). Corrosion in cracked and uncracked concrete - influence of crack width, concrete quality and crack reopening. *Magazine of Concrete Research*, *62*(6), 393–404. https://doi.org/10.1680/macr.2010.62.6.393
Park, S., & Andrawes, B. (2025). Application of NiTiNb shape memory alloys in the end region of prestressed concrete bridge girders. *Advances in Structural Engineering*. https://doi.org/10.1177/13694332251340717
Pérez-Claros, E., & Andrawes, B. (2025). Experimental Testing of Concrete Crossties Prestressed with Shape Memory Alloys. *Journal of Transportation Engineering, Part A: Systems*, *151*(10). https://doi.org/10.1061/jtepbs.teeng-8982
Poursaee, A., & Ross, B. (2022). The Role of Cracks in Chloride-Induced Corrosion of Carbon Steel in Concrete. *Corrosion and Materials Degradation*, *3*(2), 258–269. https://doi.org/10.3390/cmd3020015
Qin, H., Yang, J., Yan, K., Doh, J. H., Wang, K., & Zhang, X. (2021). Experimental research on the spalling behaviour of ultra-high performance concrete under fire conditions. *Construction and Building Materials*, *303*. https://doi.org/10.1016/j.conbuildmat.2021.124464
Roth, M. J., Rushing, T. S., Flores, O. G., Sham, D. K., & Stevens, J. W. (2010). *Laboratory Investigation of the Characterization of Cor-Tuf Flexural and Splitting Tensile Properties*.
Sung, M., & Andrawes, B. (2021). Innovative local prestressing system for concrete crossties using shape memory alloys. *Engineering Structures*, *247*, 113048. https://doi.org/10.1016/J.ENGSTRUCT.2021.113048
Sung, M., & Andrawes, B. (2023). Topology Optimization of Continuous Precast Prestressed Concrete Bridge Girders Using Shape Memory Alloys. *Journal of Structural Engineering*, *149*(6). https://doi.org/10.1061/jsendh.steng-11999
U.S. Department of Transportation, F. H. A. (2019). Status of the Nation's Highways, Bridges, and Transit. In *Conditions & Performance 23rd Edition*. https://www.federalregister.gov/documents/2017/01/18/2017-00550/national-performance-management-measures-assessing-pavement-
U.S. Department of Transportation, F. H. A. (2025). *Bridge Condition by Highway System 2025*. National Bridge Inventory. https://www.fhwa.dot.gov/bridge/nbi/no10/condition25.cfm
Van Chanh, N. (2004). Steel Fiber Reinforced Concrete. In *Faculty of Civil Engineering Ho Chi Minh City University of Technology. Seminar Material*.
Vůjtěch, J., Ryjáček, P., Campos Matos, J., & Ghafoori, E. (2021). Iron-Based shape memory alloy for strengthening of 113-Year bridge. *Engineering Structures*, *248*. https://doi.org/10.1016/j.engstruct.2021.113231
Williams, E. M., Graham, S. S., Reed, P. A., & Rushing, T. S. (2009). *Laboratory Characterization of Cor-Tuf Concrete With and Without Steel Fibers*.

Yang, J., Peng, G. F., Zhao, J., & Shui, G. S. (2019). On the explosive spalling behavior of ultra-high performance concrete with and without coarse aggregate exposed to high temperature. *Construction and Building Materials*, *226*, 932–944. https://doi.org/10.1016/j.conbuildmat.2019.07.299

Yang, Z., Hollar, J., He, X., & Shi, X. (2010). Laboratory assessment of a self-healing cementitious composite. *Transportation Research Record*, (2142), 9–17. https://doi.org/10.3141/2142-02

Zerin, A. I., & Kasuga, A. (2022). *LCA of a challenging low carbon ultra-high durability non-metallic bridge*. https://www.researchgate.net/publication/361531387

Zhao, C., Wang, Z., Zhu, Z., Guo, Q., Wu, X., & Zhao, R. (2023). Research on different types of fiber reinforced concrete in recent years: An overview. *Construction and Building Materials*, *365*. https://doi.org/10.1016/j.conbuildmat.2022.130075

Zhao, H., & Andrawes, B. (2020). Local strengthening and repair of concrete bridge girders using shape memory alloy precast prestressing plate. *Journal of Intelligent Material Systems and Structures*, *31*(11), 1343–1357. https://doi.org/10.1177/1045389X20916793

Zhou, W., Chen, Y., Wang, K., Han, S., & Palacios Galarza, F. (2017). Experimental research on circular concrete filled stainless steel tubular truss. *Thin-Walled Structures*, *117*, 224–238. https://doi.org/10.1016/j.tws.2017.04.026

Zollo, R. F. (1997). Fiber-reinforced Concrete: an Overview after 30 Years of Development. *Cement and Concrete Compositer*, *19*, 107–122. https://doi.org/10.1016/S0958-9465(96)00046-7

7. Acknowledgements

The authors acknowledge the financial support provided for this study by the Transportation Infrastructure Precast Innovation Center (TRANS-IPIC) through the University Transportation Center program of the US Department of Transportation, Office of the Assistant Secretary for Research and Technology (OST-R) under Grant No. 69A3552348333.